Available online at www.sciencedirect.com
SCIENCE DIRECT®
Biochemical and Biophysical Research Communications 307 (2003) 600–609
BBRC
www.elsevier.com/locate/ybbrc

The solution structure of the oxidized bovine microsomal cytochrome b_5 mutant V61H☆

Chunyang Cao,[a] Qi Zhang,[a] Lin-Long Xue,[b] Jinbiao Ma,[a] Yun-Hua Wang,[b] Houming Wu,[a,*] and Zhong-Xian Huang[b,*]

[a] *State Key Laboratory of Bio-Organic and Natural Products Chemistry, Shanghai Institute of Organic Chemistry, Chinese Academy of Sciences, Shanghai 200032, PR China*
[b] *Department of Chemistry, Fudan University, Shanghai 200433, PR China*

Received 3 June 2003

Abstract

Using 1488 NOE constraints, 19 stereo-specific assignments, 13 pairs of H-bond constraints, and 140 pseudo-contact shift constraints, a family of 35 structures of bovine microsomal cytochrome b_5 mutant V61H has been obtained through the program PSEUDYANA. The family has been further refined by restrained energy minimization to give a family of final structures. The RMSD values of final structures with respect to the average structure are 0.45 ± 0.11 and 0.96 ± 0.10 Å for backbone and heavy atoms, respectively. The final $\Delta\chi_{ax}$ and $\Delta\chi_{rh}$ values are 2.34×10^{-32} and -0.67×10^{-32} m^3, respectively. The comparisons between the solution structures of mutant V61H and WT cytochrome b_5, and X-ray structure of the mutant V61H show that the global folding of the molecule in solution is unchanged and the side-chain of His61 deviates from the heme pocket and extends into the solvent like in its crystal structure. However, the helices around the heme pocket undergo outward global displacement while their local conformations are well maintained. Meanwhile, the heme ring shows a little off the heme pocket, which accounts for the lower stability of the mutant. Additionally, the axial ligand rings counterclockwise rotate around His39 N–Fe axis due to the mutation, which is confirmed by variation of the hyperfine shifts of the heme protons of V61H compared to those of WT cytochrome b_5.

Keywords: Cytochrome *b5*; Mutant V61H; Solution structure

Val61 is a conserved residue in most species of cytochrome b_5 proteins with the only exception being horse [31]. According to the X-ray structure of WT bovine microsomal cytochrome b_5 (pdb entry, 1EHB) [42], Val61 is locating at the rim of the hydrophobic pocket (Fig. 1) and is involved in the hydrophobic interaction at the interface between cytochrome b_5 and cytochrome *c*. Meanwhile, it is close to the axial ligand His63 and its side chain acts as a 'gate' restricting the access of water molecules to the heme pocket. The mutation of the residue Val61 may cause the perturbation on the hydrophobic pocket of the heme and the geometry of the axial ligand planes and the heme. Therefore, three mutants of cytochrome b_5, V61H, V61E, and V61Y, have been constructed to examine the effects of the polarity, electric charge, and volume of the substituted residues on the stability, and redox potential of the protein. Among these mutants, the X-ray structure of the V61H mutant (pdb code: 1ES1) has been determined [45]. The result shows that there is no distinct difference between the X-ray structures of V61H mutant and its WT protein (pdb code: 1EHB), except the local conformation of the residue 61. However, those

☆ *Abbreviations:* WT, wild type; Tb5, trypsin-solubilized cytochrome b_5; NMR, nuclear magnetic resonance; 1D, one-dimensional; 2D, two-dimensional; 3D, three-dimensional; DSS, 4,4-dimethyl 4-silapentane sodium sulfonate; NOE, nuclear Overhauser effect; NOESY, nuclear Overhauser effect spectroscopy; DQF-COSY, double-quantum-filtered correlation spectroscopy; TOCSY, total correlated spectroscopy; ppm, parts per million; REM, restrained energy minimization; CW, clockwise; CCW, counterclockwise; pdb, protein data bank.

* Corresponding authors. Fax: +86-21-6416-6128 (H. Wu); Fax: +86-21-65641740 (Z.-X. Huang).
E-mail addresses: hmwu@mail.sioc.ac.cn (H. Wu), zxhuang@fudan.edu.cn (Z.-X. Huang).

0006-291X/03/$ - see front matter © 2003 Elsevier Inc. All rights reserved.
doi:10.1016/S0006-291X(03)01225-7

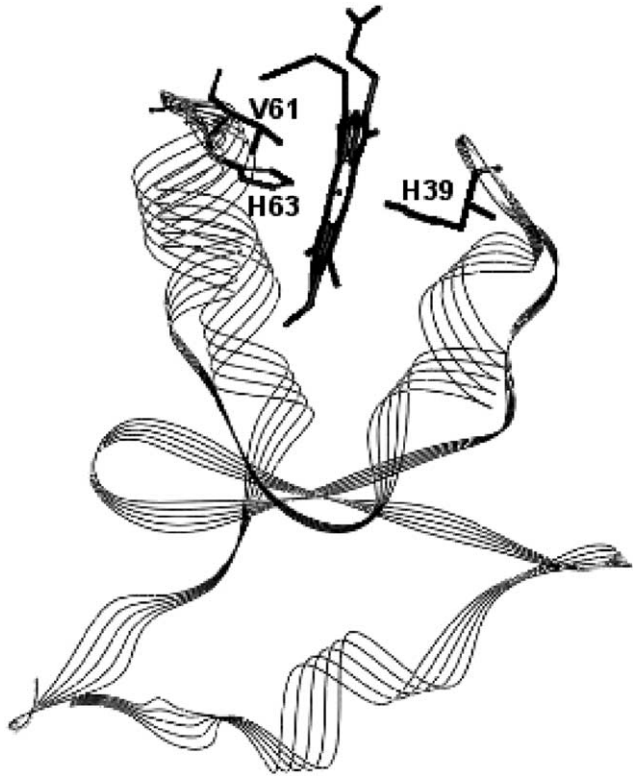

Fig. 1. The location of Val61 in WT cytochrme b_5 (pdb entry: 1EHB).

results cannot well account for the distinct variations in the NMR hyperfine shifts of the heme protons and the lower stability of the protein in solution. Herein, the 3D solution structure of the mutant V61H of bovine microsomal cytochrome b_5 has been determined by 1D and 2D ^{1}H NMR. The structural information obtained plus the hyperfine shifts of the heme protons have been used to clarify the variations of the heme hydrophobic environment and the geometry of the heme and the axial ligands.

Materials and methods

NMR sample preparation. The oxidized-state trypsin-solubilized bovine liver microsomal cytochrome b_5 mutant V61H was expressed and purified as described procedure [12]. About 12.4 mg of the protein was dissolved in 25 mM aqueous phosphate buffer in 90% H_2O and 10% D_2O, and the pH of the solution was carefully adjusted to 7.0. The final concentration was approximately 2.9 mM. The sample in D_2O was prepared by lyophilizing the sample in H_2O two times and then dissolving it in 99.96% D_2O.

NMR spectroscopy. ^{1}H NMR spectra were acquired on a Varian unity Inova600 spectrometer operating at a proton Larmor frequency of 600.14 MHz. To detect connectivities among hyperfine-shifted signals, NOESY spectrum [27,28] with a spectral width of 53 ppm in both frequency dimensions, with a recycle time of 100 ms and mixing time of 30 ms, was acquired. To optimize the detection of connectivities in the diamagnetic region (about −3.5 to 12.5 ppm), NOESY spectra were acquired with recycle time of 1.5 ms and mixing times of 50, 100, 150, and 200 ms, respectively. TOCSY [10] spectra were obtained using the spin-lock times of 30, 50, and 80 ms in H_2O and D_2O, respectively. DQF-COSY [13,37] spectra were recorded in H_2O and D_2O. WATERGATE pulse [36] sequence was used for water signal suppression in NOESY spectra in H_2O, while in other cases pre-saturation was used. All data consisted of 4K data points in the acquisition dimension and 1K experiments in the indirect dimension. Raw data were weighted with a squared cosine function, zero-filled, and Fourier-transformed to obtain a final matrix 4096×4096 data points. All spectra were collected at 293 K either on the H_2O or on the D_2O samples, processed using the Varian software VNMR (version 6.1B) on SUN ULTRA workstation, and analyzed on SGI Indigo II workstation through the XEASY program [15].

Constraints used in structure calculations. Intensities of dipolar connectivities were converted into upper distance limits, which were used as input for structure calculations. Volumes measured on NOESY maps acquired with different mixing times were calibrated simultaneously using a scaling factor for the intensities of well-defined and isolated peaks in one spectrum with respect to the other through program CALIBA [19]. Calibration curves were adjusted iteratively as the structure calculations proceeded. In the final calibration, volumes were found to be proportional to $1/r^6$. Stereospecific assignments were obtained through program GLOMSA [19] on the preliminary calculated structures.

Hydrogen-bond constraints were introduced for the un-exchanged backbone amide protons (such as NH^{23}, NH^{24}, NH^{25}, NH^{29}, NH^{30}, NH^{31}, NH^{32}, and NH^{76}, which were identified in DQF-COSY acquired in D_2O) and the distance between the NH proton and the hydrogen-bond acceptor was constrained to be in the 1.8–2.2 Å interval by inclusion of the corresponding upper and lower distance limits in structure calculation. In addition, upper limits of 3.2 Å between the N and the acceptor atoms were also included. All hydrogen-bond constraints were found to be within hydrogen-bond distance and to have the correct orientation with respect to hydrogen-bond acceptors in structure models obtained without inclusion of these constraints. These H-bond constraints are meaningful for the β-sheet determination.

Pseudo-contact shifts (pcs) were used as additional constraints in the calculation and given by [23]:

$$\delta^{\mathrm{pcs}} = \frac{1}{12\pi r_i^3}\left[\Delta\chi_{\mathrm{ax}}(3n_i^2 - 1) + \frac{3}{2}\Delta\chi_{\mathrm{rh}}(l_i^2 - m_i^2)\right]. \quad (1)$$

Therein $\Delta\chi_{\mathrm{ax}}$ and $\Delta\chi_{\mathrm{rh}}$ are the axial and rhombic magnetic susceptibility anisotropies, r_i is the length of the nuclei i from the metal ion, and l_i, m_i, and n_i are the direction cosines of the position vector of atom i with respect to orthogonal reference system formed by the principle axes of the magnetic susceptibility tensor. The pseudo-contact shifts were obtained by subtracting the shifts of the reduced form, which was estimated for the WT protein [41], from the observed chemical shifts of the oxidized form of the variant V61H. Because the reduced WT was used as a model to calculate the pcs, to avoid the calculation errors caused by the mutation, no pcs constraints were introduced for the residue that was mutated and for its neighboring residues. Meanwhile, no pcs restraints were used for the heme and the axial heme ligands (His39 and His63) that experienced a non-negligible contact shift. Using a preliminary family of 35 conformers coming from DYANA and pcs as the input files, $\Delta\chi_{\mathrm{ax}}$ and $\Delta\chi_{\mathrm{rh}}$ of each member of the family were obtained through the program FANTASIAN [5,7]. The averaged values of $\Delta\chi_{\mathrm{ax}}$ and $\Delta\chi_{\mathrm{rh}}$ were taken as starting values in the PSEUDYANA structure calculation. An upper distance limit of 0.2 Å was set between the pseudo-atom defining the origin of the magnetic anisotropy tensor and the iron atom of the heme residue. The location of this residue and the tensor orientation were optimized during the structure calculations until the final values deviated no more than 5% from the initial ones.

Structure calculations. The structure was calculated using the modified program DYANA (version 1.5) [20]. It contains the program PSEUDYANA [8], which made it suitable for the incorporation of pcs restraints. A preliminary family of 35 conformers was obtained using NOE constraints, hydrogen-bond constraints, and the pcs constraints.

Two axial ligands (His39 and His63) were coordinated to the iron atom by additional upper (2.12 Å) and lower (1.90 Å) distance limits from Nε2 atoms to the central iron atom in structure calculation. In this way, no angle is imposed between the heme plane and the His–iron bond. In particular, no assumption was made on the location of the heme group and the iron (III) ion, which were determined only by the NOEs and the pcs, respectively.

Restrained energy minimization (REM) was then applied to each member of the family by use of the AMBER Package [35]. The distance constraints were applied within the molecular mechanics and dynamics module of Sander and the pseudo-contact shifts were included as constraints by means of the module PCSHIFTS [7]. A force constant of 133.76 kJ mol^{-1} was applied for the distance constraints and of 418 kJ mol^{-1} was applied for pseudo-contact constraints.

Results

Sequence-specific assignment

Extensive lists of assignments for the oxidized cytochrome b_5 from different organisms have been reported in the literature for both the diamagnetic part of the protein [16–18,39] and hyperfine-shifted signals of the heme moiety [3,4,26]. In many cases, there are two forms in solution due to two conformations of heme ring differing by a 180° rotation around the meso-α,γ axis [21,32]. However, under our experimental condition, the system was homogeneous and only one form was observed in the solution. Therefore, the sequential assignment of the protein resonances can be achieved readily without the interference from the minor isomer signals. The obtained assignments are extended to about 78% of the total protons including those of the heme and all residues but Ala3 (data shown in supporting materials). About 80% of the present assignments are consistent with the data reported in the literature for oxidized bovine cytochrome b_5 [16,40]. However, some amino acid residues, especially those close to the heme and the mutation site, exhibit different chemical shifts. The assignment data were involved in supporting materials.

Secondary structures from NMR data

The elements of secondary structure were identified by interpreting the pattern of assigned NOEs [43]: the helical structures were identified by a number of sequential and medium-range connectivities such as $d_{\mathrm{NN}}(i,i+1)$, $d_{\mathrm{NN}}(i,i+2)$, $d_{\alpha\mathrm{N}}(i,i+3)$, $d_{\alpha\mathrm{N}}(i,i+4)$, and $d_{\alpha\beta}(i,i+3)$, while β strands were assigned by strong $d_{\alpha\mathrm{N}}$ sequential and intra-residue connectivities and long range d_{NN} and $d_{\alpha\mathrm{N}}$ connectivities. Short- and medium-range NOE networks in this protein are summarized in Fig. 2, from which five elements of helical secondary structure were identified. They involve residues 9–16 (α1), 32–39 (α2), 43–49 (α3), 55–61 (α4), and 64–75 (α5), similar to the helical secondary structural elements present in all cytochrome b_5 crystal and solution structures [1,6,14,34,38,42], except for the length of a few helices. The amide protons NH^{59}, NH^{60}, NH^{61}, NH^{72}, and NH^{73} in helices IV and V were partially exchanged. The pattern of long-range NOEs (data not shown) revealed the existence of a β sheet centered on two antiparallel β strands (residues 21–25 and 28–32), the former being parallel to the segment 51–54, and the latter antiparallel to the region 75–79. Besides, a parallel β sheet was also observed for the segments 78–80 and 5–7, respectively. In these regions, the amide protons NH^{23}, NH^{24}, NH^{25}, NH^{29}, NH^{30}, NH^{31}, NH^{32}, and NH^{76} were non-exchanged amide protons, which are consistent with tight elements of β secondary structure.

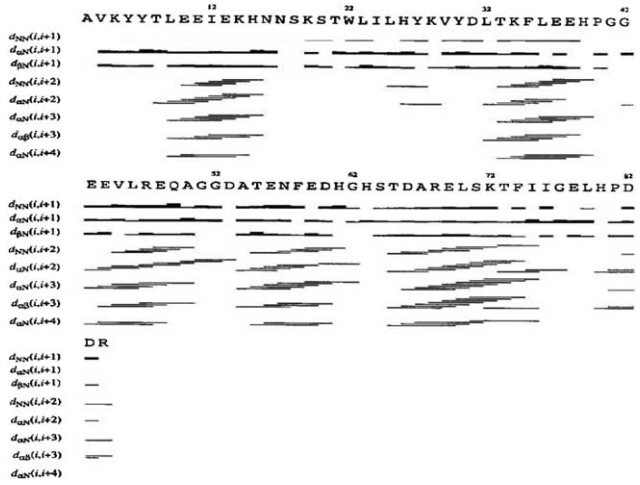

Fig. 2. Schematic representation of the sequential and medium-range NOE connectivities involving HN, H_α, and H_β for the oxidized form of cytochrome b_5 mutant V61H. The thickness of the bar indicates the intensity of NOEs.

Solution structure

A total of 1488 NOE distance constraints, 19 stereospecific assignments, 13 pairs of hydrogen-bond constraints, and 140 pseudo-contact shift constraints, were used in structure calculation. The relative weight of all kinds of constraints above was kept equal. Two hundred random structures were annealed in 15,000 steps with the above constraints. A family of 35 structures obtained from PSEUDYANA with the lowest target function has the RMSD values of 0.43 ± 0.09 and 1.05 ± 0.09 Å for backbone and heavy atoms, respectively (calculated for residue 5–80). The target function lies in the range 0.1–0.2 Å^2 (average target function of 0.16 ± 0.02 Å^2). Twelve iterations of PSEUDYANA calculation were performed before the magnetic anisotropy tensor reached convergence. Then, the family of the structures was subjected to further refinement with the program AMBER [35]. The restrained energy minimization (REM) yields a family with an average distance penalty function of 33.48 ± 3.11 kJ mol^{-1}

(28.09–42.01 kJ mol^{-1}). The resulting family has the RMSD values of 0.45 ± 0.11 and 0.96 ± 0.10 Å for backbone and heavy atoms, respectively. Fig. 3A shows the solution average structure of the family represented as a tube whose radius is proportional to the RMSD of the family, which is characterized by high resolution, even in regions close to the paramagnetic center. The RMSD values per residue for the backbone and heavy atoms are reported in Fig. 3B.

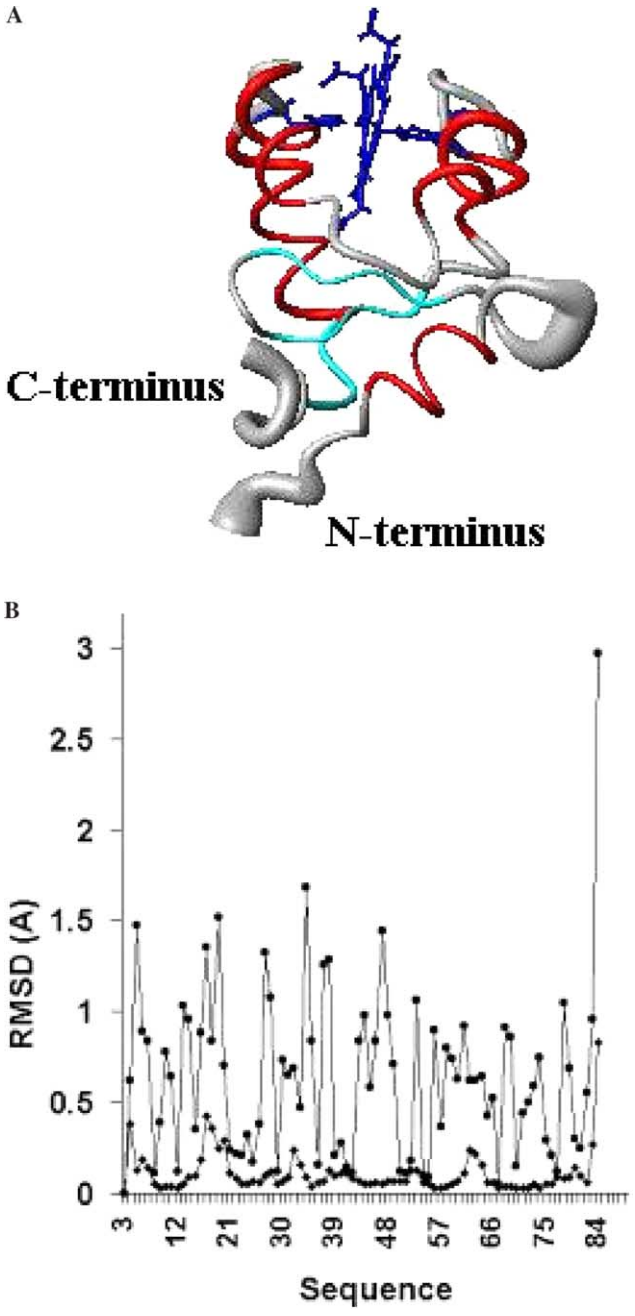

Fig. 3. (A) A family of REM structures of cytochrome b_5 mutant V61H. The figure was generated with the program MOLMOL [22] and the radius of the tube is proportional to the RMSD. (B) RMSD per residue to the mean structure for the REM family. (■) and (○) represent RMSD values per residue for backbone and for all heavy atoms, respectively.

The quality of the structure in terms of stereochemical parameters was evaluated using the programs PROCHECK [24,33] and PROCHECK_NMR [25]. According to these programs, the helical structure elements involve residues 9–14 (α1), 34–38 (α2), 43–49 (α3), 55–60 (α4), and 65–74 (α5). The assignment of all helices is similar to those identified by NOE pattern. However, similar to the solution structures of WT bovine and rat cytochrome b_5 [6,34], the length of helix α2 is shorter than that (residue 32–39) in crystal and cannot be classified as a canonical helix [29]. The short segment involving the C-terminus residues 82–84, which was the helix α6 (82–84) in crystal structure (pdb entry: 1EHB), also exhibited a helical structure in some conformations of the family. A three stranded anti-parallel β sheet was identified by PROCHECK in the region of residues 22–25, 28–31, and 75–78, former two of which are slightly shorter than those found through NOE pattern. The segment residues 6–7 and 51–54, which are parts of β1 and β4 presented in the X-ray structures of WT bovine cytochrome b_5 and its variant V61H, also appeared as β strands in some conformations of the family. The parameters describing the quality of the structure are summarized in Table 1. Low forbidden van der Waals contacts, low H-bond energy, and the overall *G*-factor larger than −0.5 were observed in the family, which indicated a good quality of the present solution structure.

The chemical shifts of heme protons

The assignment of the heme resonances was achieved by self-assistant analysis of NOE correlations according to the substitution pattern of the protons in heme structure, and the results are shown in Table 2.

The magnetic susceptibility tensor

The final $\Delta\chi_{ax}$ and $\Delta\chi_{rh}$ values are 2.34×10^{-32} and -0.67×10^{-32} m^3, respectively. They are a little different from those previously reported in the literature for rat and rabbit cytochrome b_5 ($\Delta\chi_{ax} = 2.83 \times 10^{-32}$, $\Delta\chi_{rh} = -1.06 \times 10^{-32}$ m^3; $\Delta\chi_{ax} = 2.66 \times 10^{-32}$, $\Delta\chi_{rh} = -0.91 \times 10^{-32}$ m^3) [2,9] and bovine cytochrome b_5 four-site mutant ($\Delta\chi_{ax} = 2.71 \times 10^{-32}$, $\Delta\chi_{rh} = -1.07 \times 10^{-32}$ m^3) [44]. The principal *z*-axis of the magnetic susceptibility tensor is nearly aligned to the perpendicular to the mean heme plane, making an angle of 5° with it. The *x*-axis of the magnetic susceptibility tensor makes an angle of 24.4° with the N (pyrrole II)–N (pyrrole IV) direction.

Once the magnetic susceptibility anisotropy tensor is available, it is possible to separate the contact and pseudo-contact contributions to the hyperfine shifts of the heme substituents and of the ligand protons. The results are shown in Table 3.

Table 1
Calculation statistics and structure analysis for solution structure of cytochrome b_5 mutant V61H

	Average over the family	REM mean structure
RMS violation per experimental distance constraints (Å)[a]		
Intra-residue (281)	0.0221 ± 0.0020	0.0212
Sequential (362)	0.0281 ± 0.0020	0.0337
Medium range[b] (361)	0.0305 ± 0.0022	0.0286
Long range (484)	0.0204 ± 0.0018	0.0208
Total (1488)	0.0255 ± 0.0013	0.0265
Average number of violations per structure		
Intra-residue (281)	5.3429 ± 0.5827	5.00
Sequential (362)	22.6000 ± 2.5657	26
Medium range[b] (361)	21.7429 ± 2.5110	18
Long range (484)	18.6857 ± 2.9739	21
Total (1488)	68.3714 ± 5.2322	70
Violations larger than 0.3 Å	0.1143 ± 0.3182	0
Violations between 0.1 and 0.3 Å	33.4286 ± 3.1558	36
Target function (Å^2)	0.16 ± 0.02	0.16
AMBER force field average total energy (kJ mol^{-1})	-5272 ± 33	−5208
Structure precision (Å)[c]		
Backbone	0.45 ± 0.11	—
All heavy atoms	0.96 ± 0.10	—
Structure analysis[d]		
% of residues in most favored regions	75.25 ± 0.59	75.0
% of residues in additionally allowed regions	19.24 ± 0.66	18.1
% of residues in generously allowed regions	1.60 ± 0.21	4.2
% of residues in disallowed regions	3.47 ± 0.27	2.8
No. of bad contacts/100 residues	0.11 ± 0.05	1
H-bond energy (kJ mol^{-1})	3.19 ± 0.15	3.26
Overall *G*-factor	-0.36 ± 0.007	−0.37

[a] The number of meaningful constraints for each class is reported in parentheses.
[b] Medium range distance constrains are those between residues $(i, i+2)$, $(i, i+3)$, $(i, i+4)$, and $(i, i+5)$.
[c] RMSD values are calculated for residues 5–80.
[d] The programs PROCHECK and PROCHECK-NMR were used to check the overall quality of the structure and GLY and Pro are excluded from the Ramachandran analysis. For the PROCHECK statistic, less than 10 bad contacts per 100 residues, an average hydrogen-bond energy in the range 2.5–4.0 kJ mol^{-1}, and an overall *G*-factor larger than −0.5 are expected for a good quality structure.

Discussion

To date, the solution structure and X-ray structure (pdb code: 1EHB, [45]) of mutant V61H as well as the solution structure (pdb code: 1NX7, data not published) of Tb5 WT protein are available (data not published), which allow a thorough comparison between relevant structures. A number of structural variations are uncovered and discussed as follow.

Variation in the heme hydrophobic pocket

Figs. 4A and B exhibit the superimposed diagrams (residues from 5 to 80) of the REM mean structure of V61H (black)/X-ray structure of V61H (deep gray), and REM mean structure of V61H (black)/solution structure of WT cytochrome b_5 (gray), respectively. These two diagrams demonstrate the essential identity in the secondary structure and global folding between them. However, Fig. 4B clearly shows a bit of outward global displacement of four helices around the heme pocket in V61H solution structure, meanwhile the rest parts of the structures are superimposed well.

Table 4 listed the RMSD values between the solution structures of WT cytochrome b_5 and its mutant V61H for the corresponding secondary structures in regions of 5–7, 9–14, 22–25, 28–31, 33–38, 43–49, 51–52, 55–60, 65–74, and 75–78, when the backbone of the residues 5–80 superimposed (Fig. 4B). Except for those of the fragments 5–7 and 9–14, where the relatively larger RMSD values may result from the local conformational change of the N-terminal of the protein, the RMSD values for the segment 33–38, 43–49, 55–60, and 65–74 (α-helices) are larger than those for the segment 22–25, 28–31, 51–52, and 75–87 (β-elements). This fact indicated that the mutation on Val61 leads to a bit outwards global displacement of the helices around the heme moiety in the solution structure. In other words, these helical structures are maintained well, but the backbones shifted slightly away from the heme center after mutation.

Table 2
The observed chemical shifts (ppm) for WT cytochrome b_5 and its mutant V61H in D_2O, 25 mM phosphate buffer, pH 7.00, and 293 K, reference against DSS

Protons	V61H	Tb5
1-Me	8.17	11.96
2-α-H	25.63	28.02
2-β_c-H	−7.08	−7.11
2-β_t-H	−7.60	−7.41
meso-α-H	−4.20	−3.19
3-Me	17.21	14.08
4-α-H	5.67	4.85
4-β_t-H	2.48	2.30
meso-β-H	9.57	9.10
5-Me	16.19	22.21
6-α_1-H	13.43	15.74
6-α_2-H	14.83	16.03
6-β_1-H	−1.64	−0.81
6-β_2-H	−1.88	−1.66
meso-γ-H	−1.26	−0.23
7-α_1-H	21.15	18.95
7-α_2-H	0.13	
7-β_1-H	−3.40	−3.69
7-β_2-H	1.40	1.55
8-Me	3.96	2.37
meso-δ-H	10.39	9.72

The structural variations disclosed above reflect the broadening of the heme cavity due to the mutation.

Meanwhile, Fig. 4C demonstrates that the heme moiety in the solution structure of the mutant shifts slightly towards up-left direction of the heme pocket compared to the solution structure of WT protein. In addition, there are differences in the side chain conformation of the 7-propionate of the heme between two solution structures, which can be demonstrated by the torsion angle defined by the carbonyl carbon, α- and β-carbon of the 7-propionate, and C at the 7 position of the heme. The torsion angles for the mutant and WT protein solution structures are 67.6° and 49.2°, respectively. The bigger torsion angle in the mutant indicated that the heme is up-leftwards shifting, meanwhile keeping the hydrogen bonding between 7-propionate and Ser64. The fact that the heme shifts away from the heme center clearly infers the weakening of the hydrophobic interaction between the heme and protein matrix in comparison with that of WT Tb_5.

Variation in the orientation of two axial ligand planes

Fig. 4C also shows the comparison of the orientations of two axial ligands between solution structures of V61H and its WT protein. The torsion angle between His39 imidazole ring and Fe–pyrrol II N axis is −39.1° in the solution structure of WT protein, while it was −24.8° in the solution structure of V61H. This suggests that the imidazole ring of His39 rotates CCW 14.3° about the heme normal in view from His39. The torsion angles between His63 imidazole ring and Fe–pyrrol II N axis are 32.0° in Tb_5 solution structure and 25.9° in V61H solution structure, respectively, indicating a rotation of the imidazole ring of His63 by 6.1° in the same direction. Therefore, the ϕ angles between the average plane of two axial ligands and Fe–pyrrol II N axis in the solution structures of V61 mutant and its WT protein are 25.3° and 35.6°, respectively. The average plane of two axial ligands of the mutant rotates CCW around 10.3°.

The orientation of the average imidazole plane of the axial ligands can be correlated to the hyperfine shifts of the heme protons in cytochrome b_5 proteins. According to La Mar and coworker's interpretation [26], the variation of the spread of the α, γ-*meso*-H to β, δ-*meso*-H shifts as a function of the orientation of the heme relative to fixed rhombic magnetic axes, changing at a rate of approximate 0.2 ppm/°. The shift spread of methyls in V61H (13.25 ppm) was smaller than that of WT cytochrome b_5 (18.47 ppm), while that of *meso*-Hs in V61H (14.59 ppm) was larger than that of WT cytochrome b_5 (12.33 ppm). These experimental data reveal that heme has rotated CW about its normal after the mutation from Val61 to His61. Furthermore, the mean spread of α,γ-*meso*-H to β,δ-*meso*-H defined as Δmeso is 12.71 and 11.07 ppm for V61H and WT, respectively. Therefore, the increase of Δmeso by 1.60 ppm from WT to V61H indicated the clockwise rotation of the heme about its normal by approx. 8° in the mutant, which is consistent with the value above obtained from the solution structure.

The further evidences for the geometry of the heme and the orientation of the axial ligands came from the observed shifts of heme methyls and *meso*-H. From an inspection of the data in Table 2, it is easy to obtain the pattern of hyperfine shift changes of heme protons in V61H when compared with WT cytochrome b_5. With respect to the heme methyls, the spread of the chemical shifts became smaller than that in WT. Conversely, the *meso*-H spread is larger in V61H than that in WT protein. As shown in Table 2, the average shifts (9.73 ppm) of methyls in V61H are smaller than that (12.65 ppm) of WT cytochrome b_5, and the average shifts (3.63 ppm) of *meso*-Hs in V61H are also smaller than that (4.01 ppm) of WT cytochrome b_5. It is clear that the results in this paper are consistent with the prediction made by La Mar and his co-workers. The changes in these average shifts in the mutant are essentially attributed to the decrease in spin density delocalization from Fe (III) to heme 3e(π) molecular orbitals, which is in turn correlated to the orientation angle ϕ of the average axial histidine planes.

The orientation of the side chain of the residue His61

It has been reported that the side-chain of His61 in X-ray structure of mutant V61H deviates away from the

Table 3
Separation of the contact and pseudo-contact contribution to the hyperfine shift for bovine oxidized cytochrome b_5 mutant V61H

Atom name	Res. name	Chemical shift (oxidized) (ppm)[a]	Chemical shift (reduced) (ppm)[b]	Hyperfine shift (ppm)	Calculated pseudo-contact (ppm)[c]	Contact shift (ppm)
HN	His^{39}	9.14	5.99	3.15	0.56 ± 0.10	2.59
Hα	His^{39}	6.73	2.44	4.29	1.31 ± 0.26	2.98
Hβ1	His^{39}		0.80		1.32 ± 0.27	
Hβ2	His^{39}	7.38	0.39	6.99	1.01 ± 0.26	5.98
Hδ1	His^{39}				1.40 ± 0.66	
Hε1	His^{39}				3.40 ± 2.40	
Hδ2	His^{39}				7.89 ± 1.72	
HN	His^{63}	11.40	5.98	5.42	0.64 ± 0.24	4.78
Hα	His^{63}	7.64	2.57	5.07	0.27 ± 0.32	4.80
Hβ1	His^{63}	10.12			0.67 ± 0.36	
Hβ2	His^{63}	9.60			0.64 ± 0.39	
Hδ1	His^{63}				1.68 ± 0.50	
Hε1	His^{63}		0.76		6.25 ± 1.56	
Hδ2	His^{63}				2.34 ± 1.55	
8-CH_3	heme	3.96	3.65	0.31	0.24 ± 0.26	0.07
δ-meso	heme	10.39			1.99 ± 0.75	
1-CH_3	heme	8.17	3.27	4.90	0.28 ± 0.24	4.62
2-Hα	heme	25.63	7.38	18.25	-1.70 ± 0.13	19.95
2-Hβ(t)	heme	−7.60	5.40	−13.00	-0.61 ± 0.06	−12.39
2-Hβ(c)	heme	−7.08	5.05	−12.13	-0.55 ± 0.12	−11.58
α-meso	heme	−4.20	9.27	−13.47	-4.68 ± 0.38	−8.79
3-CH_3	heme	17.21	3.36	13.85	-1.52 ± 0.21	15.37
4-Hα	heme	5.67	8.26	−2.59	0.38 ± 0.28	−2.97
4-Hβ(t)	heme	2.47	6.03	−3.56	0.23 ± 0.16	−3.79
4-Hβ(c)	heme		5.94		0.16 ± 0.24	
β-meso	heme	9.57	9.77	−0.20	1.94 ± 0.71	−2.14
5-CH_3	heme	16.19	3.49	12.70	0.26 ± 0.23	12.44
β-meso	heme	−1.26	9.30	−10.56	-4.65 ± 0.39	−5.91
7-$H\alpha_1$	heme	21.15	4.29[d]	16.86	-1.85 ± 0.21	18.71
7-$H\alpha_2$	heme	0.13	4.11[d]	−3.98	-0.91 ± 0.18	−3.07
7-$H\beta_1$	heme	−3.40			-1.16 ± 0.16	
7-$H\beta_2$	heme	1.40			-0.91 ± 0.20	
6-$H\alpha_1$	heme	13.43	4.00[d]	9.43	-0.95 ± 0.13	10.38
6-$H\alpha_2$	heme	14.83	3.82[d]	11.01	-1.99 ± 0.16	13.00
6-$H\beta_1$	heme	−1.87			-1.14 ± 0.17	
6-$H\beta_2$	heme	−1.64			-0.54 ± 0.11	

[a] Resonance assignments are obtained at 293 K in 20 mM phosphate buffer.
[b] The shift of the reduced species is taken from the work published by Banci et al. [11].
[c] The calculated pseudo-contact shift is the average of the shifts calculated over each number of the family of the conformers constituting structure.
[d] Since stereo-specific assignment for the propionate diastereotopic pairs is not available for all protons, the average chemical shift of each methylene pair in the reduced form was taken as diamagnetic reference.

heme pocket and extended into the solvent [45]. Fig. 4D are the superimposed diagram of the 61st residue while superimposing (from 5 to 80) the secondary structures of the REM mean structure of the mutant V61H (black), X-ray structure of V61H (deep gray), and REM solution structure of WT cytochrome b_5 (gray) at a time. The RMSD values of backbone atoms of 61st residue are 0.03 ± 0.00 Å for V61H REM structure, 0.01 ± 0.01 Å for the X-ray of V61H, and 0.02 ± 0.02 Å for WT cytochrome b_5, respectively. These data indicate that the backbone atoms of 61st residue in these three structures superimposed well. Superimposing the solution structure and X-ray structure of V61H, the RMSD for heavy atoms of His61 is 0.45 Å, and for backbone atoms 0.02 Å, suggesting that the orientation of the side-chain of His61 in solution structure is the same as that in X-ray of V61H. From Fig. 4D, it is clear that the extending direction of His61 imidazole ring in both X-ray and solution structures of V61H variant locates in the original position of γ_2-CH_3 of residue Val61 in WT cytochrome b_5. In the solution structure of V61H, the side-chain of His61 imidazole makes an angle 41.5° with the heme plane, which is slightly different from that (37.8°) in the X-ray structure. The space left by the angle displacement plus the idle position of the original γ_1-CH_3 of residue Val61 may form a solvent-exposed area, which results in the decrease of the hydrophobicity of the heme pocket.

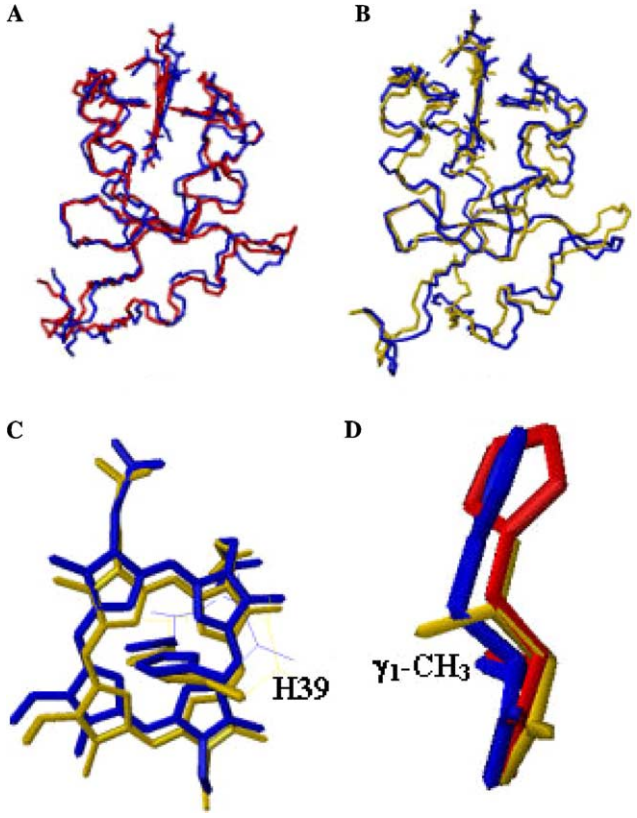

Fig. 4. (A) Superimposed diagram of cytochrome b_5 mutant V61H REM mean structure (black) and X-ray structure (1ES1) of V61H (deep gray). (B) Superimposed diagram of cytochrome b_5 mutant V61H REM mean structure (black) and the WT REM mean structure (gray). (C) The location of the heme and the orientation of the axial ligands. (D) Superimposed diagram of 61st residue backbone of the REM mean structure of mutant V61H (black), X-ray structure of V61H (1ES1, deep gray), and solution structure of WT cytochrome b_5 (1NX7, gray).

Table 4
Comparison between solution structures of Tb5 and V61H and X-ray structure of V61H (backbone of 5–80 was superimposed)

Peptide chain	V61H REM + Tb5 REM		V61H X-ray +V61H REM	
	bb (Å)	Heavy (Å)	bb (Å)	Heavy (Å)
9–14	0.36	1.47	0.34	1.53
33–38	0.31	1.57	0.47	2.51
43–49	0.28	1.42	0.21	1.29
55–60	0.33	1.46	0.11	1.09
65–74	0.80	1.50	0.66	1.17
5–7	0.70	1.69	0.57	1.25
22–25	0.23	0.53	0.19	0.73
28–31	0.33	1.18	0.19	0.94
51–52	0.15	0.20	0.23	0.39
75–78	0.24	0.61	0.17	0.46

The stability of V61H mutant

As mentioned in the previous report [45], the stability of the variant V61H towards heat and urea is much lower than that of the WT cytochrome b_5. Generally, the stability of cytochrome b_5 is attributed to two respects: (1) The stability of the secondary and the tertiary structures of the protein. (2) The interaction between the heme and the protein matrix: the tighter it is, the more stable the protein. The comparison made above between the solution structure of V61H and WT Tb_5 indicated that there was no remarkable difference in the secondary structure and the tertiary structure of the proteins. Thus, the lower stability of the variant V61H should come from the interaction between the heme and its pocket. As discussed previously, the formation of the solvent-exposed area on the heme pocket due to the alteration of the side chain by the mutation from Val to His results in increase of the accessibility of water to the heme pocket. The side-chain of His61 in the mutant solution points out of the pocket, which may lead to the forming, a "gate" of the water channel into the hydrophobic pocket. The change of the hydrophobicity of the heme pocket reduces the interaction between the heme and its pocket, and results in the broadening of the heme pocket. Therefore, the structural variations in the solution structure uncovered by current study offer a reasonable explanation for the lower stability of the V61H mutant.

The redox potential of V61H

Investigations on electron transferring in this system showed that the redox potential of the mutant is positively shifted by 21 mV and its rate of electron transfer becomes slower [45]. In the present system, the decrease in hydrophobicity of the heme pocket of the mutant may move the reduction potential negatively. Besides, in the mutant, the average plane of two axial ligands rotated CCW by about 10.3°. This may decrease the spin density delocalization from Fe (III) to heme 3e(π) molecular orbitals, thus, resulting in reduction potential moving negatively. However, it was reported that the electrostatic potential around the heme-exposed area dominates the redox potential of the heme proteins [26,30,45]. In the case of a negatively charged protein such as cytochrome b_5, the increasing of positive charge at the heme-exposed surface always stabilizes reduced state of the iron ion, making the redox potential shift positively. For the mutant V61H, a positive charge was introduced into the heme pocket by the residue His61. Therefore, decreasing of the density of negative charge in heme-exposed area leads to the redox potential moving positively.

On the other hand, the electron transferring behavior of the heme proteins could be correlated to the molecular recognition between redox partners. As demonstrated previously, the variations in the hydrophobic pocket and the heme location, as well as conformation of the propionate on the heme, will influence the dock-

ing of the redox partner participating in the electron transferring process, and in turn slowing up the electron transferring between them.

Supporting materials

Table S1: Chemical Shifts of the ^{1}H of the mutant V61H.

Data deposition

The codes of the solution structures of the WT cytochrome b_5 and its mutant V61H in Protein Data Bank (PDB) are 1NX7 and 1J0Q.

Acknowledgments

This project was supported by the National Science Foundation of P.R. China (No. 20132030), Chinese Academy of Sciences, and State Minister of Science and Technology. The authors are indebted to the Institute of Molecular Biology and Biophysics, ETH-Hönggerberg Zürich, Switzerland, for the programs CALIBA, DYANA (version 1.5) and XEASY; Prof. Bertini of Florence University, Italy, for the programs PSEUDYANA and PCSHIFT; Prof. James W. Caldwell of California University, for the program AMBER (version 5.0); and Prof. Wen-Xia Tang, Dr. Gaohua Liu, and Dr. Yibing Wu of Nanjing University, China, for helpful discussion. We also thank Tripos Inc. for the SYBYL software.

References

[1] P. Argos, F.S. Mathews, The structure of ferrocytochrome b5 at 2.8 Å resolution, J. Biol. Chem. 250 (1975) 747–751.
[2] F. Amesano, L. Banci, I. Bertini, I.C. Felli, The solution structure of oxidized rat microsomal cytochrome b_5, Biochemistry 37 (1) (1998) 173–184.
[3] L. Banci, R. Pierattelli, A.J. Vila, 1H-13C HETCOR investigations on heme-containing systems, Inorg. Chem. 33 (19) (1994) 4338–4343.
[4] L. Banci, R. Pierattelli, D.L. Turner, Determination of haem electronic structure in cytochrome *b*5 and metcyanomyoglobin, Eur. J. Biochem. 232 (1995) 522–527.
[5] L. Banci, I. Bertini, K.L. Bren, M.A. Cremonini, H.B. Gray, C. Luchinat, P. Turano, The use of pseudocontact shifts to refine solution structures of paramagnetic metalloproteins: Met80Ala cyano-cytochrome *c* as an example, J. Biol. Inorg. Chem. 1 (2) (1996) 117–126.
[6] L. Banci, I. Bertini, F. Ferroni, A. Rosato, Solution structure of reduced microsomal rat cytochrome *b*5, Eur. J. Biochem. 249 (1997) 270–279.
[7] L. Banci, I. Bertini, G. Gori Savellini, A. Romagnoli, P. Turano, M.A. Cremonini, C. Luchinat, H.B. Gray, Pseudocontact shifts as constraints for energy minimization and molecular dynamics calculations on solution structures of paramagnetic metalloproteins, PROTEINS: Struct. Funct. Genet. 29 (1) (1997) 68–76.
[8] L. Banci, I. Bertini, M.A. Cremonini, G. Gori Savellini, C. Luchinat, K. Wuthrich, P. Guentert, PSEUDYANA for NMR structure calculation of paramagnetic metalloproteins using torsion angle molecular dynamics, J. Biomol. NMR 12 (4) (1998) 553–557.
[9] L. Banci, I. Bertini, A. Rosato, S. Scaacchier, Solution structure of oxidized microsomal rabbit cytochrome b_5, Eur. J. Biochem. 267 (3) (2000) 755–766.
[10] A. Bax, D.G. Davis, MLEV-17 based two-dimensional homonuclear magnetization transfer spectroscopy, J. Magn. Reson. 65 (1985) 355–360.
[11] I. Bertini, C. Luchinat, G. Parigi, F.A. Walker, Heme methyl ^{1}H chemical shifts as structural parameters in some low-spin ferriheme proteins, J. Biol. Inorg. Chem. 4 (1999) 515–519.
[12] D.L. Brautigan, S.F. Miller, E. Margoliash, Mitochondrial cytochrome *c*: preparation and activity of native and chemically modified cytochrome *c*, Methods Enzymol. 53D (1978) 128–164.
[13] A.E. Derome, M.P. Williamson, Rapid-pulsing artifacts in double- quantum-filtered COSY, J. Magn. Reson. 88 (1990) 177–185.
[14] R.C.E. Durley, F.S. Mathews, Refinement and structural analysis of bovine cytochrome *b*5 at 1.5 Å resolution, Acta. Crystallogr. D 52 (1996) 65–76.
[15] C. Eccles, P. Guntert, K. Wuthrich, Efficient analysis of protein 2D NMR spectra using the software package *EASY*, J. Biomol. NMR 1 (1991) 111–130.
[16] R.D. Guiles, J. Atman, I.D. Kuntz, L. Waskell, J.J. Lipka, Structural studies of cytochrome *b*5; complete sequence-specific resonance assignments for the trypsin-solubilized microsomal ferrocytochrome *b*5 obtained from pig and calf, Biochemistry 29 (5) (1990) 1276–1289.
[17] R.D. Guiles, V.J. Basus, I.D. Kuntz, L. Waskell, Sequence-specific proton and nitrogen-15 resonance assignments for both equilibrium forms of the soluble heme binding domain of rat ferrocytochrome *b*5, Biochemistry 31 (46) (1992) 11365–11375.
[18] R.D. Guiles, V.J. Basus, S. Sarma, S. Malpure, K.M. Fox, I.D. Kuntz, L. Waskell, Novel heteronuclear methods of assignment transfer from a diamagnetic to a paramagnetic protein: application to rat cytochrome *b*5, Biochemistry 32 (32) (1993) 8329–8340.
[19] P. Guntert, W. Braun, K. Wuthrich, Efficient computation of three-dimensional protein structures in solution from nuclear magnetic resonance data using the program DIANA and the supporting program CALIBA, HABAS and GLOMSA, J. Mol. Biol. 217 (1991) 517–530.
[20] P. Guntert, C. Mumenthaler, K. Wuthrich, Torsion angle dynamics for nmr structure calculation with the new program DYANA, J. Mol. Biol. 273 (1) (1997) 283–298.
[21] R.M. Keller, K. Wüthrich, Structural study of the heme crevice in cytochrome *b*5 based on individual assignment of ^{1}H NMR lines of the heme group and selected amino acid residues, Biochem. Biophys. Acta 621 (1980) 204–217.
[22] R. Koradi, M. Billeter, K. Wuthrich, MOLMOL: a program for display and analysis of macromolecular structure, J. Mol. Graphics. 14 (1996) 51–55.
[23] R.J. Kurland, B.R. McGarvey, Isotropic NMR shifts in transition metal complexes: calculation of the Fermi contact and pseudocontact terms, J. Magn. Reson. 2 (1970) 286–301.
[24] R.A. Laskowski, M.W. MacArthur, D.S. Moss, J.M. Thornton, A program to check the stereochemical quality of protein structures, J. Appl. Crystallogr. 26 (1993) 283–291.
[25] R.A. Laskowski, J.A.C. Rullmann, M.W. MacArthur, R. Kaptein, J.M. Thornton, AQUA and PROCHECK_NMR: programs for checking the quality of protein structures solved by NMR, J. Biomol. NMR 8 (1996) 477–486.
[26] K.B. Lee, G.N. La Mar, K.E. Mansfield, K.M. Smith, T.C. Pochapsky, S.G. Sligar, Interpretation of hyperfine shifts patterns in ferricytochrome *b*5 in terms of angular position of the heme: a sensitive probe for peripheral heme protein interactions, Biochem. Biophys. Acta 1202 (1993) 189–199.
[27] S. Macura, K. Wuthrich, R.R. Ernst, The relevance of J cross-peaks in two-dimensional NOE experiments of macromolecules, J. Magn. Reson. 47 (1982) 351–357.

[28] D. Marion, K. Wuthrich, Application of phase sensitive two-dimensional correlated spectroscopy (COSY) for measurements of ^{H}–^{H} spin–spin coupling constants in proteins, Biochem. Biophys. Res. Commun. 113 (1983) 967–974.
[29] F.S. Mathews, M. Levine, P. Argos, Three-dimensional fourier synthesis of calf liver cytochrome *b*5 at 2.8 Å resolution, J. Mol. Biol. 64 (1972) 449–464.
[30] F. Mathews, E. Czerwinski, in: A. Martonosi (Ed.), The Enzymes of Biological Membranes, Wiley, New York, 1976, pp. 143–147.
[31] F.S. Mathews, The structure, function and evolution of cytochromes, Prog. Biophys. Mol. Biol. 45 (1985) 1–56.
[32] S.J. Mclachlan, G.N. La Mar, P.D. Burns, K.D. Smith, K.C. Langry, ^{1}H NMR assignment and the dynamics of interconversion of the siomeric forms of cytochrome *b*5 in solution, Biochem. Biophys. Acta 874 (1986) 274–284.
[33] A.L. Morris, M.W. MacArthur, E.G. Hutchinson, J.M. Thornton, Stereochemical quality of protein structure coordinates, PROTEINS: Struct. Funct. Genet. 12 (1992) 345–364.
[34] F.W. Muskett, G.P. Kelly, D. Whitford, The solution structure of bovine ferricytochrome b_5 determined using heteronuclear NMR methods, J. Mol. Biol. 258 (1) (1996) 172–189.
[35] D.A. Pearlman, D.A. Case, J.W. Caldwell, W.S. Ross, T.E. Cheatham, D.M. Ferguson, G.L. Seibel, U.C. Singh, P.K. Weiner, P.A. Kollman, AMBER 5.0, University of California, San Francisco, CA, 1997.
[36] M. Piotto, V. Saudek, V. Sklenar, Gradient-tailored excitation for single-quantum NMR spectroscopy of aqueous solutions, J. Biomol. NMR 2 (1992) 661–666.
[37] M. Rance, O.W. Sorensen, G. Bodenhausen, G. Wagner, R.R. Ernst, K. Wuthrich, Improved spectral resolution of COSY^{H} NMR spectra of proteins via double quantum filtering, Biochem. Biophys. Res. Commun. 117 (1983) 479–485.
[38] M.J. Rodriguez-Maranon, F. Qiu, R.E. Stark, S.P. White, X. Zhang, S.I. Foundling, V. Rodriguez, C.L. Schilling, R.A. Bunce, M. Rivera, ^{13}C NMR spectroscopic and X-ray crystallographic study of the role played by mitochondrial cytochrome b_5 heme propionates in the electrostatic binding to cytochrome, Biochemistry 35 (50) (1996) 16378–16390.
[39] S. Sarma, R.J. Digate, D. Banville, R.D. Guiles, ^{1}H, ^{13}C and ^{15}N NMR assignments and secondary structure of the paramagnetic form of rat cytochrome *b*5, J. Biomol. NMR 8 (1996) 171–183.
[40] Y.L. Sun, Y.H. Wang, M.M. Yan, B.Y. Sun, Y. Xie, Z.X. Huang, S.K. Jiang, H.M. Wu, Structure, interaction and electron transfer between cytochrome b_5, its E44A and/or E56A mutants and cytochrome *c*, J Mol. Biol. 285 (1) (1999) 347–359.
[41] N.C. Veitch, D. Whitford, R.J.P. Williams, An analysis of pseudocontact shifts and their relationship to structural features of the redox states of cytochrome b_5, FEBS Lett. 269 (2) (1990) 297–304.
[42] J. Wu, J.H. Gan, Z.X. Xia, Y.H. Wang, W.H. Wang, L.L. Xue, Y. Xie, Z.X. Huang, Crystal structure of recombinant trypsin-solubilized fragment of cytochrome b_5 and the structural comparison with Val61His mutant, PROTEINS: Struct. Funct. Genet. 40 (2) (2000) 249–257.
[43] K. Wuthrich, in: K. Wuthrich (Ed.), NMR of Proteins and Nucleic Acids, Wiley, New York, 1986, p. 162.
[44] Y.B. Wu, Y.H. Wang, C.M. Qian, J. Lu, E. Li, W.H. Wang, J.X. Lu, Y. Xie, J.F. Wang, D.X. Zhu, Z.X. Huang, W.X. Tang, Solution structure of cytochrome b_5 mutant (E44/48/56A/D60A) and its interaction with cytochrome, Eur. J. Biochem. 268 (6) (2001) 1620–1630.
[45] L.L. Xue, Y.H. Wang, Y. Xie, P. Yao, W.H. Wang, W. Qian, Z.X. Huang, J. Wu, Z.X. Xia, Effect of mutation at valine 61 on the three-dimensional structure, stability, and redox potential of cytochrome b_5, Biochemistry 38 (1999) 11961–11972.